# Large Rayleigh number thermal convection: Heat flux predictions and strongly nonlinear solutions

Gregory P. Chini[1,a)] and Stephen M. Cox[2]
[1]*Department of Mechanical Engineering, University of New Hampshire, Durham, New Hampshire 03824, USA*
[2]*School of Mathematical Sciences, University of Nottingham, Nottingham NG7 2RD, United Kingdom*

(Received 17 September 2008; accepted 28 July 2009; published online 26 August 2009)

We investigate the structure of strongly nonlinear Rayleigh–Bénard convection cells in the asymptotic limit of large Rayleigh number and fixed, moderate Prandtl number. Unlike the flows analyzed in prior theoretical studies of infinite Prandtl number convection, our cellular solutions exhibit dynamically inviscid constant-vorticity cores. By solving an integral equation for the cell-edge temperature distribution, we are able to predict, as a function of cell aspect ratio, the value of the core vorticity, details of the flow within the thin boundary layers and rising/falling plumes adjacent to the edges of the convection cell, and, in particular, the bulk heat flux through the layer. The results of our asymptotic analysis are corroborated using full pseudospectral numerical simulations and confirm that the heat flux is maximized for convection cells that are roughly square in cross section. © *2009 American Institute of Physics*. [DOI: 10.1063/1.3210777]

## I. INTRODUCTION

Boussinesq thermal convection in a horizontal layer between isothermal stress-free boundaries is the archetypal convection problem and has served as a prime testing ground for the development of new theoretical understanding. In both natural and technological applications, the Rayleigh number (Ra) generally exceeds the threshold for linear instability of the conduction state by orders of magnitude, so the high-Ra limit of the governing equations is of particular interest. It is therefore remarkable that the asymptotic structure of steady-state convection cells has not yet been established, except in the further limiting case of infinite Prandtl number[1] (Pr). This situation is rectified in the present paper: we provide the first large-Ra asymptotic analysis of the classical Rayleigh–Bénard convection problem with $\mathrm{Pr}=O(1)$ in which both details of the flow and a corresponding bulk heat transport coefficient, as a function of the cell aspect ratio, are systematically derived.

At high Rayleigh number, observed convective motions are, of course, turbulent, so the practical, rather than academic, interest of the present study warrants further discussion. To this end, we note that there is growing evidence from numerical simulations and laboratory experiments of the intermittent occurrence of spatially coherent states in a range of canonical turbulent flows (including free convection and channel and pipe flows[2]). These coherent states appear to correspond to saddles in phase space; although they are unstable, their attracting directions lead to their recurring presence in observations. Furthermore, the coherent flow patterns often can be identified with simple exact solutions of the governing equations possessing a high degree of symmetry. For instance, in simulations[3,4] and experiments[5] of (even weakly) sheared convection, coherent roll vortices arise intermittently which resemble the two-dimensional (2D) convection cells analyzed in this work. Although detailed connections are not made here, we believe that our analysis of laminar but strongly nonlinear convection ultimately may play a role in shedding light on turbulent heat transport in high-Ra flows.

Significant progress has been made in prior large-Ra asymptotic analyses of Rayleigh–Bénard convection cells by restricting attention to the infinite-Pr limit, which is often motivated by reference to the exceedingly high Prandtl numbers [e.g., $\mathrm{Pr}=O(10^{23})$] in mantle convection. Busse *et al.*,[6] for example, have recently analyzed mantle convection between two low-viscosity layers, but they do not explicitly treat the vertical plumes and thermal boundary layers of interest here. Of particular relevance to the present investigation is the analysis of Jimenez and Zufiria,[1] who considered infinite-Pr convection between isothermal stress-free horizontal boundaries. Building on the earlier efforts by Roberts[7] and Olson and Corcos,[8] Jimenez and Zufiria proceeded[1] by demonstrating that the core of the convection cell is to a good approximation isothermal (see, e.g., Ref. 9); they then examine in detail the thermal boundary layers adjacent to the edges of the cell. In particular, they resolve the solution near the corners where the thin rising and falling plumes along the vertical edges of the cell join to the boundary layer flows along the horizontal walls and confirm that these corner regions are dynamically passive. This conclusion enables them to formulate an integral equation for the temperature distribution around the perimeter of the cell. By solving the integral equation, Jimenez and Zufiria are able to explicitly compute the proportionality coefficient (as a function of cell aspect ratio) in the asymptotic relationship between Nusselt and Rayleigh numbers—by construction, the Nusselt number associated with their cellular solutions scales in proportion to the Rayleigh number to the one-third power. The correspond-

a)Author to whom correspondence should be addressed. Tel.: 001 603 862 2633. FAX: 001 603 862 1865. Electronic mail: greg.chini@unh.edu.

 

ing calculation for the case of finite Prandtl number is the main goal of the present work.

A singular perturbation analysis of steady Rayleigh–Bénard convection at finite Pr seems to have first been attempted by Pillow.[10] In contrast to the formulation given here for stress-free boundaries, however, an *ad hoc* approach was adopted to analyze the boundary layers along no-slip upper and lower walls. Robinson[11] improved upon Pillow's study by correctly treating the flow in the dynamically inviscid and passive corners, but even for the stress-free case, his calculation of the boundary layer structure similarly involved certain *ad hoc* approximations not invoked in the present investigation. Nevertheless, several key ideas in our singular perturbation analysis were first correctly given in Robinson's study.

Further discussion of the relevant background has been provided by one of us in Ref. 12, where the related problem of thermal convection between fixed-heat-flux horizontal boundaries is treated, along with the mathematically analogous problem of Langmuir circulation, a wind- and wave-driven convective flow in the upper ocean. In the interests of brevity, that background material is not repeated here.

The remainder of the paper is organized as follows. In Sec. II, we set out the mathematical problem to be solved for 2D large-Ra steady convection. In Sec. III, we present large-Ra numerical simulations of the corresponding initial value problem, which converge at large times to steady convection cells, to motivate the principal features of the solution assumed in the asymptotic analysis of Sec. IV. From this asymptotic solution, we show in Sec. V how to compute the heat flux across the fluid layer. As in the work of Jimenez and Zufiria, it is necessary to solve numerically an integral equation for the cell-edge temperature distribution to determine the heat flux. Given the asymptotic scalings which are adopted, only a single constant (albeit dependent on the cell aspect ratio) need be computed from the solution to this integral equation. Results for the flow and the consequent heat flux are given in Sec. VI.

## II. PROBLEM FORMULATION

We consider the 2D Oberbeck–Boussinesq equations governing Rayleigh–Bénard convection at $O(1)$ Prandtl number with Dirichlet conditions imposed on the temperature along the upper and lower horizontal boundaries. Using a stream function/vorticity representation, these equations can be expressed in nondimensional form as

$$\frac{\partial T}{\partial t}+\frac{\partial \psi}{\partial z}\frac{\partial T}{\partial y}-\frac{\partial \psi}{\partial y}\frac{\partial T}{\partial z}=\epsilon^2\nabla^2 T, \tag{1}$$

$$\frac{\partial \Omega}{\partial t}+\frac{\partial \psi}{\partial z}\frac{\partial \Omega}{\partial y}-\frac{\partial \psi}{\partial y}\frac{\partial \Omega}{\partial z}=\mathrm{Pr}\,\epsilon\frac{\partial T}{\partial y}+\mathrm{Pr}\,\epsilon^2\nabla^2\Omega, \tag{2}$$

$$\nabla^2\psi=-\Omega. \tag{3}$$

Here $T$ is the total temperature field, $\psi$ is the streamfunction describing the cellular flow in the $y-z$ plane, and $\Omega$ is the corresponding $x$-directed vorticity component. Equations (1)–(3) have been nondimensionalized using $H$, the depth of the convective layer, to scale distances; $\Delta T$, the temperature drop imposed across the layer, to scale the temperature; and $U\equiv(\kappa/H)\mathrm{Ra}^{2/3}$ to scale the cellular velocity components. The dimensionless parameter $\mathrm{Ra}\equiv\alpha\Delta T g H^3/\nu\kappa$ is the Rayleigh number, where $\alpha$ is the thermal expansion coefficient, $g$ the gravitational acceleration, $\nu$ the kinematic viscosity and $\kappa$ the thermal diffusivity. $\mathrm{Pr}\equiv\nu/\kappa$ is the Prandtl number. We are interested in solutions to Eqs. (1)–(3) in the limit of large Ra or, equivalently, small $\epsilon$, where

$$\epsilon\equiv\mathrm{Ra}^{-1/3}.$$

Motivated in part by convection occurring in geophysical boundary layers (e.g., the ocean surface mixed layer), we impose stress-free boundary conditions along the upper and lower boundaries of the convection zone ($z=0$ and $z=-1$, respectively), where we also require the vertical velocity component to vanish. Here we treat the canonical problem of Rayleigh–Bénard convection with constant-temperature boundary conditions; the analogous problem of thermal convection with constant-heat-flux boundary conditions has been analyzed in Ref. 12. Thus,

$$T(y,0,t)=0,\quad \Omega(y,0,t)=0,\quad \psi(y,0,t)=0, \tag{4}$$

$$T(y,-1,t)=1,\quad \Omega(y,-1,t)=0,\quad \psi(y,-1,t)=0. \tag{5}$$

We seek steady cellular solutions exhibiting discrete translational invariance in the horizontal coordinate $y$ and reflection symmetry about the planes $y=n\pi/k$ for integer $n$ and given cell width $\pi/k$. Thus, we impose the following symmetry conditions on the lateral cell boundaries:

$$\frac{\partial T}{\partial y}(0,z,t)=0,\quad \Omega(0,z,t)=0,\quad \psi(0,z,t)=0, \tag{6}$$

$$\frac{\partial T}{\partial y}(\pi/k,z,t)=0,\quad \Omega(\pi/k,z,t)=0,\quad \psi(\pi/k,z,t)=0. \tag{7}$$

Note that the horizontal wavenumber $k$ of the convection pattern appearing in Eq. (7) must be specified as an input parameter (but see Sec. VI); the analysis given below then provides the corresponding large-Ra asymptotic form for the convection.

For fixed-temperature boundary conditions, a useful global diagnostic of the strength of the convection is the normalized heat flux (more properly, heat flow rate) through the layer, i.e., the Nusselt number,

$$\mathrm{Nu}=\frac{Q}{\rho c\kappa\Delta T\pi/k}, \tag{8}$$

where $c$ is the coefficient of specific heat of the fluid and $Q$ is the dimensional heat flow rate (per unit length in the $x$ direction) through the upper or lower boundary. In general, $\mathrm{Nu}=\mathrm{Nu}(\mathrm{Ra},\mathrm{Pr},k)$. The large-Ra scaling behavior of Nu is of particular interest and a subject of some controversy. Indeed, there is no universally accepted empirical large-Ra scaling or theoretical prediction for what the scaling should be.[13] Proposed values of the scaling exponent $\beta_T$ in the presumed power-law relation $\mathrm{Nu}\sim\mathrm{Ra}^{\beta_T}$ include the "classical" value[14–18] $\beta_T=1/3$ and the nonclassical value[19–24] $\beta_T=2/7$.

Rigorous bounds on Nu have been obtained using upper-bound analysis and modern variational methods. For arbitrary Pr, the best known bound[24–27] is $\beta_T = 1/2$ (i.e., strictly above estimates from scaling theories and experiments), although $\beta_T = 1/3$ holds (to within logarithmic corrections) for infinite Pr.[28] Discrepancies in measured or predicted values of $\beta_T$ are variously attributed to the failure to realize sufficiently large values of Ra in experiments or simulations, to differences in domain size and geometry, and to the influence of thermal and velocity boundary conditions.

The solutions considered here are found to exhibit the classical scaling[15]

$$\mathrm{Nu} = C(\mathrm{Pr},k)\mathrm{Ra}^{1/3} \quad \text{as} \quad \mathrm{Ra} \to \infty. \tag{9}$$

This scaling is appropriate for thermal convection with stress-free boundaries, as discussed here; with no-slip boundaries, there may be a transition to a different scaling at sufficiently large Ra, when the momentum boundary layers become unstable. Using asymptotic analysis, we compute the coefficient $C(\mathrm{Pr},k)$ in Eq. (9) for steady 2D cellular convection with $\mathrm{Pr} = O(1)$; numerical simulations at large but finite Ra corroborate the asymptotic analysis. Although the laminar flows we investigate are undoubtedly unstable in this limit (e.g., the 2D numerical solutions described in Sec. III are found to be unstable to long wavelength, i.e., Eckhaus, and to three-dimensional instabilities; see Ref. 29), the fact that their scaling behavior is consistent with that of (numerically) realizable turbulent flows attests to their relevance. For example, Amati *et al.*[30] performed direct numerical simulations of turbulent thermal convection at $\mathrm{Pr} = 0.7$ in a small aspect-ratio cylindrical cell with no-slip, isothermal upper and lower boundary conditions and found that $\mathrm{Nu} \sim \mathrm{Ra}^{1/3}$ from $\mathrm{Ra} = 10^{10}$ to $\mathrm{Ra} = 10^{14}$. Furthermore, our solutions exhibit certain flow features observed in experiments and numerical simulations of turbulent convection, including isothermal mean core temperature distributions and plumes emanating from thermally unstable boundary layers and spanning the layer depth (e.g., see Fig. 2 of Ref. 13, where high-resolution direct numerical simulations of 2D Rayleigh–Bénard convection are described). This observed similarity, and the similar physical mechanisms involved, suggests that these solutions may provide insights into the structure of turbulent convection, although a proper analysis of their presumed role as saddles in phase space[2] lies well beyond the scope of the present work.

## III. NUMERICAL SIMULATIONS

We have carried out time-dependent numerical simulations of Eqs. (1)–(3) subject to boundary conditions (4)–(7) using a pseudospectral collocation method. To provide adequate resolution of the narrow boundary layers and plumes, a Chebyshev tensor-product formulation was employed (see, e.g., Ref. 31). For certain simulations, a rational mapping was used to further cluster grid points in the viscous and thermal layers around the cell edge. In this way, we ensured that these layers were well resolved, typically with no fewer than nine grid points, in all of the simulations reported here. A semi-implicit time discretization scheme was employed, with the nonlinear and instability terms advanced using a second-order Adams–Bashforth method, and the linear diffusive terms advanced using the trapezium rule. The resulting linear algebraic system was solved by direct matrix inversion.

For $\mathrm{Ra} = O(10^6)$, $\mathrm{Pr} = O(1)$, $k = O(1)$, and a range of initial conditions, steady-state cellular solutions were obtained. Figure 1 shows one example computed with $k = \pi$, $\mathrm{Pr} = 1$, and $\epsilon = 0.01$. Several features of these solutions are exploited in the asymptotic analysis described in Sec. IV. In particular, we note that both the (scalar) vorticity and temperature fields are strongly homogenized in the core of the convection cell, with thin viscous and thermal layers arising along the cell edge. This behavior is well known in various contexts[1,12,32–34] and can be expected on theoretical grounds (see Sec. IV). The existence of boundary layers, narrow plumes, and uniform core temperature distributions distinguishes these laminar but strongly nonlinear convection cells from their weakly nonlinear counterparts. Indeed, linear instability of the nonconvecting base state occurs at $\mathrm{Ra} = O(10^3)$ (and at precisely[35] $\mathrm{Ra} = 27\pi^4/4 \approx 657.5$ for $k = \pi/\sqrt{2}$). Nevertheless, even under strongly supercritical forcing, the stream function is everywhere smooth, as evident in Fig. 1. This smoothness is attributable to the usual increased smoothness of solutions to a Poisson equation such as Eq. (3) (relative to the smoothness of the inhomogeneous term, i.e., the vorticity, on the right-hand side), particularly under the imposed stress-free boundary and symmetry conditions.

## IV. ASYMPTOTIC ANALYSIS OF FULLY NONLINEAR SOLUTIONS

Motivated by the results of the numerical simulations, we use matched asymptotic analysis to obtain a semianalytical description of steady cellular convection in the small-$\epsilon$ (i.e., large-Ra), $O(1)$-Pr limit. As shown in Fig. 2, the cell is broken into various subdomains, including a dynamically inviscid vortex core, upper and lower vorticity and thermal boundary layers, corner regions, and vertical plumes along the lateral edges of the cell. These subdomains are characterized by different dominant balances of terms in Eqs. (1)–(3). The corners are not discussed in detail here, except to note that: (i) in an "outer" corner region having an $O(\epsilon^{1/2})$ length scale in both $y$ and $z$, $T(y,z)$ and $\Omega(y,z)$ are passively advected between the boundary layers and plumes;[12] (ii) the commensurate $O(\epsilon^{1/2})$ horizontal and vertical scales are required to ensure that volume fluxes can be matched between the boundary layers and corners and between the corners and plumes (note that the flow in the boundary layers and plumes slows as the corner stagnation points are approached), see pp. 135–136 of Ref. 36; and (iii) inner diffusive corner sublayers must arise to accommodate the change in boundary conditions on $T(y,z)$ as the flow traverses the corners.

Although the asymptotic analysis given here closely parallels the analysis for the constant-heat-flux case given in Ref. 12, several differences are noteworthy. First, when the heat flux is held fixed, convection largely eradicates the temperature jump across the fluid layer induced by conduction alone; i.e., the temperature variation across the thermal lay-

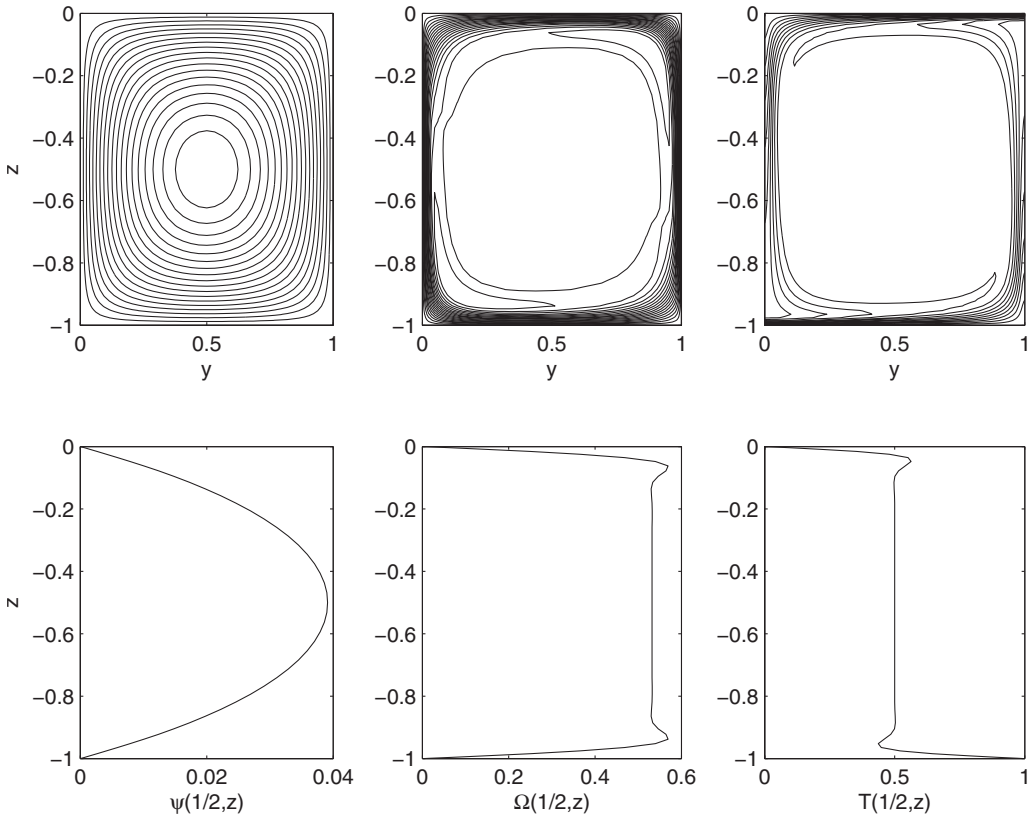


FIG. 1. Upper row: contour plots of (from left to right) $\psi(y,z)$, $\Omega(y,z)$, and $T(y,z)$, computed numerically using a pseudospectral method for $\epsilon=0.01$ (i.e., $\mathrm{Ra}=10^6$), $k=\pi$, and $\mathrm{Pr}=1$. Lower row: corresponding vertical profiles $\psi(1/2,z)$, $\Omega(1/2,z)$, and $T(1/2,z)$. The steady-state solutions illustrated here are representative of laminar, strongly nonlinear convection at large Ra.

ers and plumes is asymptotically small. In contrast, since an $O(1)$ temperature jump across the layer is imposed in the present study, there is a concomitant $O(1)$ temperature change across the thermal layers and plumes. Nevertheless, in both scenarios advection dominates buoyancy forcing *except* in narrow plumes because the flow is fast when Ra is large.

Next, for fixed-temperature boundary conditions, the core vorticity, which controls the strength of the cellular flow, and the heat flux through the layer must be determined simultaneously. (When the flux is specified, the coupling necessarily is only one way.[12]) Although this introduces no substantial conceptual difficulties, the analysis is complicated if an iterative approach is employed to compute these quantities. Jimenez and Zufiria[1] faced a similar difficulty in their analysis of infinite-Pr convection, although the core vorticity is not homogenized in that case. We follow their lead by introducing a modified small parameter,

$$\varepsilon \equiv (\sigma/\mathrm{Ra})^{1/3}. \tag{10}$$

The nondimensional parameter,

$$\sigma \equiv \left(\frac{\mathrm{Ra}}{\mathrm{Nu}^3}\right)^{1/4}, \tag{11}$$

is related to the (*a priori* unknown) heat flux through the layer, but is an $O(1)$ constant provided that the scaling relationship (9) holds. In terms of $\varepsilon$, the steady-state version of Eqs. (1)–(3) used in the subsequent analysis becomes

$$\frac{\partial\psi}{\partial z}\frac{\partial T}{\partial y}-\frac{\partial\psi}{\partial y}\frac{\partial T}{\partial z}=\varepsilon^2\nabla^2 T, \tag{12}$$

$$\frac{\partial\psi}{\partial z}\frac{\partial\Omega}{\partial y}-\frac{\partial\psi}{\partial y}\frac{\partial\Omega}{\partial z}=\sigma\,\mathrm{Pr}\,\varepsilon\frac{\partial T}{\partial y}+\mathrm{Pr}\,\varepsilon^2\nabla^2\Omega, \tag{13}$$

$$\nabla^2\psi=-\Omega. \tag{14}$$

The occurrence of $\sigma$ in Eq. (13) renders this formulation inappropriate for numerical simulations, but obviates the need for iteration in the asymptotic calculation of the heat flux—see Secs. IV C and V.

The most significant difference between the constant-flux and constant-temperature analyses is that in the former case the resulting "Childress[32] cell problem" can be (formally) reduced to a quadrature, while in the latter it yields an integral equation. For reasons articulated in Sec. V, the accurate numerical solution of this integral equation is a challenging task.

### A. Vortex core

In the small-$\varepsilon$ (i.e., weak-diffusion) limit, the steady-state temperature distribution is uniform in the vortex core. The homogenization of scalar fields by steady 2D cellular flows, sometimes referred to as "flux expulsion" since field gradients are suppressed, has been discussed by various authors; see, e.g., Ref. 9. To demonstrate the uniformity of $T$ in

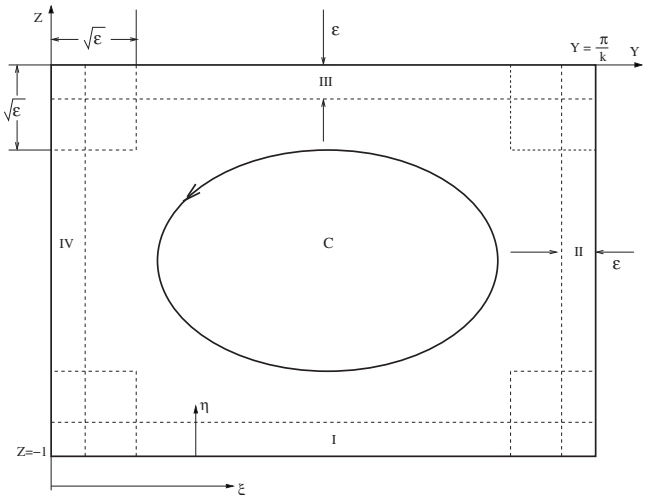


FIG. 2. Hypothesized multiregion asymptotic structure of a steady Rayleigh–Bénard convection cell as $\varepsilon \propto \epsilon \to 0$ (or $\mathrm{Ra} \to \infty$). Region $C$ is the dynamically inviscid vortex core; regions I and III are $O(\varepsilon)$-thick thermal and vorticity boundary layers; and regions II and IV are up- and downwelling plumes, respectively, also of thickness $O(\varepsilon)$. The temperature and vorticity fields are passively advected through the outer corner regions, characterized by commensurate $O(\sqrt{\varepsilon})$ horizontal and vertical scales. $\xi$ is a stretched arc-length coordinate running around the cell perimeter and $\eta$ is a scaled coordinate measuring distance normal to the thermal boundary layers and plumes.

the core, we write Eq. (12) in conservative form, integrate over the area inside a closed streamline $C_\psi$, and use the divergence theorem to yield

$$\varepsilon^2 \oint_{C_\psi} \frac{\partial T}{\partial n} dl = 0, \tag{15}$$

where $dl$ is an element of arc length along the streamline and $\partial T/\partial n$ is a normal derivative. Assuming that there exists a family of streamlines on which $T$ is smoothly varying in the small-$\varepsilon$ limit, Eq. (12) implies that $T=T(\psi)$ in that region. Substitution into Eq. (15) then yields $\varepsilon^2 T'(\psi)\Gamma_c=0$, where the prime denotes ordinary differentiation and $\Gamma_c$ is the nonzero circulation around $C_\psi$. Thus, $T \sim \bar{T}$ in the vortex core, where $\bar{T}=1/2$ by symmetry. We note that $T \sim 1/2$ trivially satisfies Eq. (12) to all algebraic orders in $\varepsilon$. In Sec. IV B, we shall show, further, that no corrections algebraic in $\varepsilon$ are forced in the interior by the diffusive layers around the cell perimeter, since $T(y,z)$ satisfies a diffusion equation there (in rescaled and transformed coordinates).

A similar argument can be used to demonstrate the homogenization of $\Omega(y,z)$ in the vortex core, as we now illustrate. In momentum form, the steady Oberbeck–Boussinesq equations can be written as

$$\boldsymbol{\omega} \times \mathbf{v} = -\boldsymbol{\nabla}\left(\mathcal{P} + \tfrac{1}{2}|\mathbf{v}|^2\right) + \sigma\,\mathrm{Pr}\,\varepsilon(T - T_B(z))\hat{\mathbf{z}} + \mathrm{Pr}\,\varepsilon^2\nabla^2\mathbf{v}. \tag{16}$$

Here, $\mathbf{v}=v\hat{\mathbf{y}}+w\hat{\mathbf{z}}$ is the 2D velocity vector, with components $v$ and $w$ in the $y$ and $z$ directions, respectively, $\boldsymbol{\omega}=(\partial w/\partial y - \partial v/\partial z)\hat{\mathbf{x}} \equiv \Omega\hat{\mathbf{x}}$ is the vorticity vector, $\mathcal{P}$ is the deviation of the pressure from the hydrostatic distribution of the nonconvecting base state, and $T_B(z)=-z$ is the linear base state temperature profile. Taking the scalar product of Eq. (16) with $d\mathbf{l}$, an infinitesimal arc-length vector tangent to a closed streamline $C_\psi$, and integrating around that streamline yields, after some manipulation, the following exact result:

$$-\sigma \oint_{C_\psi} z\,\boldsymbol{\nabla} T \cdot d\mathbf{l} = \varepsilon \oint_{C_\psi} \left(\frac{\partial \Omega}{\partial z}\hat{\mathbf{y}} - \frac{\partial \Omega}{\partial y}\hat{\mathbf{z}}\right) \cdot d\mathbf{l}. \tag{17}$$

Physically, Eq. (17) indicates that, as a fluid particle completes a circuit around a streamline, the net work done by the buoyancy force is balanced by frictional dissipation. Since $T \sim \bar{T}$ to all algebraic orders in $\varepsilon$ away from the diffusive layers, the right-hand side of Eq. (17) also must be zero to all orders in $\varepsilon$. Furthermore, if $\Omega(y,z)$ is smooth in the core, Eq. (13) implies that $\Omega \sim \Omega(\psi)$ there, as $\varepsilon \to 0$, again using $T \sim \bar{T}$. Substituting into Eq. (17) gives $\varepsilon\Omega'(\psi)\Gamma_c = o(\varepsilon^m)$ for any $m=1,2,3,\ldots$; hence, to within exponentially small corrections in $\varepsilon$, $\Omega \sim \bar{\Omega}$ in the vortex core, where $\bar{\Omega}$ is a constant (cf. Ref. 33). Unlike $\bar{T}$, however, $\bar{\Omega}$ is not known *a priori*, but instead must be determined as part of the solution (see Sec. IV C).

Using these homogenization results, we posit the following asymptotic expansions in the dynamically inviscid vortex core:

$$T \sim \bar{T} + \mathrm{E.S.T.}, \tag{18}$$

$$\Omega \sim \bar{\Omega} + \mathrm{E.S.T.}, \tag{19}$$

$$\psi \sim \psi_c(y,z) + \varepsilon\psi_c^{(1)}(y,z) + \cdots, \tag{20}$$

where E.S.T. denotes exponentially small terms in $\varepsilon$ and the subscript $c$ denotes quantities relating to the core. Substituting into Eq. (14) yields, at leading order,

$$\nabla^2\psi_c = -\bar{\Omega}, \tag{21}$$

subject to $\psi_c=0$ on $z=0,-1$ and on $y=0,\pi/k$. The solution may be expressed as the Fourier sine series,

$$\psi_c(y,z) = \sum_{n=1}^{\infty} \psi_n(z)\sin(nky), \tag{22}$$

where the sum is taken over *odd* $n$ and

$$\psi_n(z) = \frac{4\bar{\Omega}}{\pi k^2 n^3}\left\{1 - \frac{\cosh[nk(z+1/2)]}{\cosh(nk/2)}\right\}. \tag{23}$$

For subsequent matching with the bottom boundary layer ("region I") and the vertical plume along $y=\pi/k$ ("region II"), we note that

$$\psi_c(y,z) \sim (z+1)V(y) \equiv (z+1)\sum_{n=1}^{\infty}\left(\frac{4\bar{\Omega}}{\pi k n^2}\right)\tanh\left(\frac{nk}{2}\right)\sin(nky) \tag{24}$$

as $z \to -1^+$, and

$$\psi_c(y,z) \sim -(y-\pi/k)W(z) \equiv -(y-\pi/k)\sum_{n=1}^{\infty}\left(\frac{4\bar{\Omega}}{\pi k n^2}\right)\left\{1-\frac{\cosh[nk(z+1/2)]}{\cosh(nk/2)}\right\} \tag{25}$$

as $y \to \pi/k^{-}$. Again, the sums in Eqs. (24) and (25) are taken over odd $n$ only. Given the stress-free boundary and symmetry conditions, $V(y)$ and $W(z)$ are the leading-order tangential velocity components in the bottom boundary layer and the vertical plume, respectively. These functions are completely known apart from the multiplicative factor $\bar{\Omega}$, which considerably simplifies the analysis of these regions.

### B. Boundary layers and plumes

Viscous effects cannot be neglected around the perimeter of the cell, where temperature and vorticity gradients are large, owing to the mismatch between the imposed boundary and symmetry conditions and the core temperature and vorticity distributions. In the bottom boundary layer, the usual balance between normal diffusion and advection yields an $O(\varepsilon)$ layer thickness, so we introduce a rescaled vertical coordinate $Z=(z+1)/\varepsilon$. We also expand the dependent variables as

$$T(y,z) \sim \bar{T} + \theta_{\mathrm{I}}(y,Z) + \varepsilon\theta_{\mathrm{I}}^{(1)}(y,Z) + \cdots, \tag{26}$$

$$\Omega(y,z) \sim \Omega_{\mathrm{I}}(y,Z) + \cdots, \tag{27}$$

$$\psi(y,z) \sim \varepsilon\psi_{\mathrm{I}}(y,Z) + \cdots. \tag{28}$$

(By symmetry, analogous scalings apply within the upper-boundary layer.) Note from Eq. (26) that an $O(1)$ correction to $\bar{T}$ is required in the thermal boundary layer. Furthermore, although $\Omega(y,-1)=0$, the numerical simulations show that the vorticity reaches an $O(1)$ value in the core; thus, $\Omega_{\mathrm{I}}$ is an $O(1)$ function of $y$ and $Z$, to be determined. Finally, since very little fluid passes through the layer, $\psi(y,z)$ is small, $O(\varepsilon)$, in that region.

After substitution of the expansions (26)–(28) into the rescaled versions of Eqs. (12)–(14), the leading-order equation for the stream function has the solution

$$\psi_{\mathrm{I}}(y,Z) = V(y)Z, \tag{29}$$

which matches smoothly with $\psi_c(y,z)$ in the vortex core. Using Eq. (29), we find that the leading-order boundary-layer equations for $\theta_{\mathrm{I}}(y,Z)$ and $\Omega_{\mathrm{I}}(y,Z)$ linearize, a crucial simplification. Furthermore, these equations completely decouple in the thermal boundary layers because the buoyancy torque is weak relative to advection. Using Crocco (or Von Mises) coordinates, these linear, nonconstant-coefficient advection-diffusion equations can be reduced to constant-coefficient heat equations. Specifically, upon writing $\theta_{\mathrm{I}}(y,Z) \equiv \Theta_{\mathrm{I}}(s,\psi_{\mathrm{I}})$ and $\Omega_{\mathrm{I}}(y,Z) \equiv \omega_{\mathrm{I}}(s,\psi_{\mathrm{I}})$, where

$$s(y) = \int_0^y V(\tau)d\tau = \sum_{n=1}^{\infty}\left(\frac{4\bar{\Omega}}{\pi k^2 n^3}\right)\tanh\left(\frac{nk}{2}\right)[1-\cos(nky)] \tag{30}$$

(and the sum is over odd $n$), the boundary-layer equations reduce to

$$\frac{\partial\Theta_{\mathrm{I}}}{\partial s} = \frac{\partial^2\Theta_{\mathrm{I}}}{\partial\psi_{\mathrm{I}}^2}, \tag{31}$$

$$\frac{\partial\omega_{\mathrm{I}}}{\partial s} = \mathrm{Pr}\frac{\partial^2\omega_{\mathrm{I}}}{\partial\psi_{\mathrm{I}}^2}. \tag{32}$$

Equation (31) is solved subject to $\Theta_{\mathrm{I}}(s,0)=1/2$ and $\Theta_{\mathrm{I}}(s,\psi_{\mathrm{I}})\to 0$ as $\psi_{\mathrm{I}}\to\infty$. The boundary conditions for Eq. (32) are $\omega_{\mathrm{I}}(s,0)=0$ and $\omega_{\mathrm{I}}(s,\psi_{\mathrm{I}})\to\bar{\Omega}$ as $\psi_{\mathrm{I}}\to\infty$.

Analogous considerations apply in the vertical plumes, but with the roles of $y$ and $z$ reversed. In the upwelling plume along $y=\pi/k$, we set $y=\pi/k+\varepsilon Y$ and

$$T(y,z) \sim \bar{T} + \theta_{\mathrm{II}}(Y,z) + \varepsilon\theta_{\mathrm{II}}^{(1)}(Y,z) + \cdots, \tag{33}$$

$$\Omega(y,z) \sim \Omega_{\mathrm{II}}(Y,z) + \cdots, \tag{34}$$

$$\psi(y,z) \sim \varepsilon\psi_{\mathrm{II}}(Y,z) + \cdots. \tag{35}$$

Upon matching with $\psi_c(y,z)$, we find the leading-order solution for the stream function in the upwelling plume to be

$$\psi_{\mathrm{II}}(Y,z) = -W(z)Y. \tag{36}$$

The boundary-layer equations for the temperature and vorticity again linearize (see Ref. 37 for an early application of the latter result to eddies in a wake behind a bluff body). However, the buoyancy torque in the plumes is strong and balances advection and normal diffusion at leading order. Thus, the vorticity within the plume is coupled to the temperature there, although the converse is not true; i.e., the leading-order plume temperature is independent of the vorticity distribution within the plume. Upon setting $\theta_{\mathrm{II}}(Y,z) \equiv \Theta_{\mathrm{II}}(\psi_{\mathrm{II}},r)$ and $\Omega_{\mathrm{II}}(Y,z) \equiv \omega_{\mathrm{II}}(\psi_{\mathrm{II}},r)$, where

$$r(z) = \int_{-1}^{z} W(\tau)d\tau = \sum_{n=1}^{\infty}\left(\frac{4\bar{\Omega}}{\pi k n^2}\right)\left\{z+1-\frac{\tanh(nk/2)}{nk} - \frac{\sinh[nk(z+1/2)]}{nk\cosh(nk/2)}\right\} \tag{37}$$

(again summing only over odd $n$), we find that the boundary-layer equations for the temperature and vorticity are transformed to

$$\frac{\partial\Theta_{\mathrm{II}}}{\partial r} = \frac{\partial^2\Theta_{\mathrm{II}}}{\partial\psi_{\mathrm{II}}^2}, \tag{38}$$

$$\frac{\partial\omega_{\mathrm{II}}}{\partial r} = \mathrm{Pr}\frac{\partial^2\omega_{\mathrm{II}}}{\partial\psi_{\mathrm{II}}^2} - \frac{\sigma\,\mathrm{Pr}}{\mathcal{W}(r)}\frac{\partial\Theta_{\mathrm{II}}}{\partial\psi_{\mathrm{II}}}, \tag{39}$$

where $\mathcal{W}(r)=W(z)$. Equation (38) is solved subject to $\partial\Theta_{\mathrm{II}}/\partial\psi_{\mathrm{II}}=0$ on $\psi_{\mathrm{II}}=0$ and $\Theta_{\mathrm{II}}(\psi_{\mathrm{II}},r)\to 0$ as $\psi_{\mathrm{II}}\to\infty$. The

boundary conditions for Eq. (39) are $\omega_{\mathrm{II}}(0,r)=0$ and $\omega_{\mathrm{II}}(\psi_{\mathrm{II}},r)\to\bar{\Omega}$ as $\psi_{\mathrm{II}}\to\infty$.

Corresponding problems hold in the layers adjacent to the remaining two cell boundaries.

The formal solutions to the diffusion problems (31), (32), and (38) in terms of quadratures are not recorded here (but see Sec. V). The inhomogeneous solution to Eq. (39), $\omega_{\mathrm{II}p}$, is given by

$$\omega_{\mathrm{II}p}(\psi_{\mathrm{II}},r)=-\sigma\sqrt{\mathrm{Pr}}\int_0^r\int_0^\infty\frac{\frac{\partial\Theta_{\mathrm{II}}}{\partial\chi}(\chi,\rho)}{2\mathcal{W}(\rho)\sqrt{\pi(r-\rho)}}\times\left[e^{-(\psi_{\mathrm{II}}-\chi)^2/(4\,\mathrm{Pr}(r-\rho))}-e^{-(\psi_{\mathrm{II}}+\chi)^2/(4\,\mathrm{Pr}(r-\rho))}\right]d\chi d\rho. \tag{40}$$

This particular integral, which can be expressed compactly as $-\sigma[z(r)+1]\partial\Theta_{\mathrm{II}}/\partial\psi_{\mathrm{II}}$ for $\mathrm{Pr}=1$ [where $z(r)$ is the inverse of $r(z)$ in Eq. (37)], accounts explicitly for the vorticity production within the plume arising from the buoyancy torque. Note, however, that the solutions to Eqs. (31), (32), (38), and (39) are not completely specified until $\bar{\Omega}$ and appropriate upstream, or "initial," conditions are known. These issues are addressed in Secs. IV C and V, respectively.

### C. Global energy and heat flux balances

As demonstrated in Ref. 12, the core vorticity can be asymptotically estimated by making use of global energy and heat flux balances. In fact, since the temperature rather than the heat flux is specified in this investigation, the $O(1)$ parameter $\sigma$ has been *defined* so that $|\bar{\Omega}|\sim 1$, as shown below.

Multiplying Eq. (13) by $\psi$ and integrating over the domain gives the exact result,

$$\sigma\int_{-1}^0\int_0^{\pi/k}\psi\frac{\partial T}{\partial y}dydz=\varepsilon\int_{-1}^0\int_0^{\pi/k}\Omega^2dydz, \tag{41}$$

which may be interpreted as an energy balance: the rate at which the buoyancy torque does work on the cellular flow (the left-hand side) is balanced, in steady state, by the rate at which the kinetic energy of the flow is dissipated by viscous effects (the right-hand side). The latter can be easily estimated in the limit $\varepsilon\to 0$ for the laminar solution being investigated. Since $\Omega=O(1)$ everywhere in the domain, including within the boundary layers, the dominant contribution to the volume-integrated energy dissipation arises in the dynamically inviscid vortex core (a result that is well known in the context of free-surface boundary layers; see, e.g., Ref. 38). Since $\Omega\sim\bar{\Omega}$ in the core, the right-hand side of Eq. (41) is asymptotically equal to $\varepsilon\bar{\Omega}^2\pi/k$. The leading contribution to the energy production, which also must be $O(\varepsilon)$, occurs in the vertical plumes, which have an $O(\varepsilon)$ area and in which $\partial T/\partial y=O(1/\varepsilon)$ and $\psi=O(\varepsilon)$. Using the Crocco variable transformation and noting that there are two plumes, we find

$$\bar{\Omega}^2\sim-\frac{2k\sigma}{\pi}\int_{-1}^0\int_0^\infty\psi_{\mathrm{II}}\frac{\partial\Theta_{\mathrm{II}}}{\partial\psi_{\mathrm{II}}}d\psi_{\mathrm{II}}dz=\frac{2k\sigma}{\pi}\int_{-1}^0\int_0^\infty\Theta_{\mathrm{II}}d\psi_{\mathrm{II}}dz \tag{42}$$

after integrating by parts and using boundary and matching conditions.

To determine $\bar{\Omega}$, it is not necessary to know the temperature distribution across the plume, but only its integral, which is related to the *a priori* unknown heat flux through the layer. By integrating Eq. (12) over part of the cell and using the divergence theorem, the following exact result is obtained:

$$\varepsilon^2\int_0^{\pi/k}\left.\frac{\partial T}{\partial z}\right|_{z=-1}dy=\int_0^{\pi/k}\left[\varepsilon^2\frac{\partial T}{\partial z}-w(T-\bar{T})\right]_{z=z_*}dy, \tag{43}$$

where $z_*$ refers to some depth $z$ within the cell away from the thermal boundary layers. Equation (43) requires the conductive heat flux integrated across the lower boundary of the cell to be balanced, in steady state, by the sum of the advective and diffusive vertical heat fluxes integrated across the cell along $z=z_*$. Re-expressing the left-hand side in terms of $\theta_{\mathrm{I}}(y,Z)$ yields $\varepsilon\int_0^{\pi/k}\partial\theta_{\mathrm{I}}/\partial Z dy$, where the derivative is evaluated along $Z=0$. The leading contribution to the right-hand side is also $O(\varepsilon)$, again within the $O(\varepsilon)$ thick vertical plumes, where $T(y,z)-\bar{T}=O(1)$ and $w=O(1)$. Making use of these results, we find

$$\int_0^\infty\Theta_{\mathrm{II}}d\psi_{\mathrm{II}}\sim-\frac{1}{2}\int_0^{\pi/k}\left.\frac{\partial\theta_{\mathrm{I}}}{\partial Z}\right|_{Z=0}dy, \tag{44}$$

which is independent of $z$. Finally, we note that the Nusselt number is

$$\mathrm{Nu}=-\frac{k}{\pi}\int_0^{\pi/k}\left.\frac{\partial T}{\partial z}\right|_{z=-1}dy=-\frac{k}{\varepsilon\pi}\int_0^{\pi/k}\left.\frac{\partial\theta_{\mathrm{I}}}{\partial Z}\right|_{Z=0}dy; \tag{45}$$

employing this relationship together with Eqs. (10), (44), and (42), we obtain

$$|\bar{\Omega}|\sim 1. \tag{46}$$

Equation (46) is a precise asymptotic statement, not a mere order-of-magnitude estimate. Although the same result is obtained for Rayleigh–Bénard convection with constant-heat-flux boundary conditions,[12] we emphasize that the reasons are different in the two cases. When the heat flux is specified, the core vorticity is constant independently of the horizontal wavenumber $k$. In contrast, in the present case, numerical simulations show that the core vorticity, while homogenized in the small-$\varepsilon$ limit, varies with cell aspect ratio precisely because the integrated heat flux (or Nu) varies with $k$. The fact that $\bar{\Omega}$ in Eq. (46) is independent of $k$ is a consequence of the introduction of $\sigma$ into the definition of the small parameter $\varepsilon$. With $\bar{\Omega}$ given by Eq. (46) for all $k$, the stretched lengths of the boundary layers and

plumes in Crocco coordinates—$l_1 \equiv s(\pi/k)$ and $l_2 \equiv r(0)$, respectively—can be calculated. This facilitates the computation of the heat flux through the layer by obviating the need for iteration (see Sec. V). Once the flux is known, $\sigma$ can be determined and the problem is closed. Using Eqs. (9) and (11), the variation with $k$ of $\hat{\Omega}$, the steady-state core vorticity obtained by solving Eqs. (1)–(3) at a specified, large value of Ra (or $\epsilon$) rather than Eqs. (12)–(14) at the corresponding value of $\varepsilon$, is then given by the formula $|\hat{\Omega}| \sim \sigma^{-2/3}|\bar{\Omega}| = \sqrt{C(\mathrm{Pr},k)}$.

## V. CALCULATION OF THE HEAT FLUX AS A FUNCTION OF THE CELL WAVENUMBER

In this section, we follow Jimenez and Zufiria[1] in formulating and solving a Childress[32] cell problem [see Eqs. (47)–(51) below] for the cell-edge temperature distribution, and then using that solution to compute the heat flux across the convection cell. We introduce new coordinates $\xi$ and $\eta$, respectively, along and normal to the cell boundary; these are analogous to the Crocco variables which were explicitly introduced near walls I and II in Sec. IV B. [For example, near the wall at $z=-1$, $\xi - s = 0 \bmod 2(l_1+l_2)$ and $2\eta = \psi_{\mathrm{I}}$; in the ascending plume near $y=\pi/k$, $\xi - l_1 - r = 0 \bmod 2(l_1+l_2)$, and $2\eta = \psi_{\mathrm{II}}$.] In the boundary layers and plumes, $\Theta$ is defined to be the leading-order temperature field that we have previously denoted by $\bar{T}+\Theta_{\mathrm{I}}$, $\bar{T}+\Theta_{\mathrm{II}}$, etc. Note that in these coordinates $\Theta(\xi,\eta)$ is a periodic function of $\xi$, with $\Theta(\xi+L,\eta) = \Theta(\xi,\eta)$ for all $\xi$, $\eta$, where $L=2(l_1+l_2)$. In view of Eqs. (31) and (38) and the associated boundary conditions, it follows that

$$\frac{\partial \Theta}{\partial \xi} = \frac{1}{4}\frac{\partial^2 \Theta}{\partial \eta^2} \tag{47}$$

subject to

$$\Theta(\xi,0) = 1 \quad \text{for } mL < \xi < mL + l_1, \tag{48}$$

$$\frac{\partial \Theta}{\partial \eta}(\xi,0) = 0 \quad \text{for } mL + l_1 < \xi < \left(m+\frac{1}{2}\right)L, \tag{49}$$

$$\Theta(\xi,0) = 0 \quad \text{for } \left(m+\tfrac{1}{2}\right)L < \xi < \left(m+\tfrac{1}{2}\right)L + l_1, \tag{50}$$

$$\frac{\partial \Theta}{\partial \eta}(\xi,0) = 0 \quad \text{for } \left(m+\frac{1}{2}\right)L + l_1 < \xi < (m+1)L \tag{51}$$

for any integer $m$, and $\Theta(\xi,\eta) \sim 1/2$ as $\eta \to \infty$. The formal solution for $\Theta(\xi,\eta)$ can then be expressed as

$$\Theta(\xi,\eta) = \frac{1}{(\pi\xi)^{1/2}}\int_0^\infty \Theta(0,\eta')\left(e^{-(\eta-\eta')^2/\xi} - e^{-(\eta+\eta')^2/\xi}\right)d\eta' + \frac{\eta}{\pi^{1/2}}\int_0^\xi \frac{\Theta_w(\xi-p)}{p^{3/2}}e^{-\eta^2/p}dp, \tag{52}$$

where $\Theta_w(\xi) \equiv \Theta(\xi,0)$ is the temperature at the wall (i.e., around the perimeter of the cell). As Jimenez and Zufiria[1] note, the right-hand side of Eq. (52) may be rewritten by replacing $\xi$ with $\xi + mL$ for any integer $m$, in view of the periodicity of $\Theta(\xi,\eta)$ in $\xi$. In the limit as $m \to \infty$, the first integral vanishes, so that the temperature anywhere in the thermal layers is given in terms of the wall temperature by

$$\Theta(\xi,\eta) = \frac{\eta}{\pi^{1/2}}\int_0^\infty \frac{\Theta_w(\xi-p)}{p^{3/2}}e^{-\eta^2/p}dp; \tag{53}$$

the advantage of this formulation is that Eq. (53) does not depend on the unknown upstream or initial condition $\Theta(0,\eta)$. Of course, the wall temperature is known *a priori* on only two sides of the convection cell; it can be determined on the remaining walls by employing the flux boundary conditions there. First, note from Eq. (53) that the normal derivative of the temperature may be written in the form

$$\frac{\partial \Theta}{\partial \eta} = \frac{1}{\pi^{1/2}}\int_0^\infty \frac{\Theta_w(\xi-p)-\Theta_w(\xi)}{p^{3/2}}e^{-\eta^2/p}dp + \frac{1}{\pi^{1/2}}\int_0^\infty \frac{\Theta_w(\xi)-(2\eta^2/p)\Theta_w(\xi-p)}{p^{3/2}}e^{-\eta^2/p}dp. \tag{54}$$

To apply the flux boundary conditions on the vertical walls of the cell, we consider the limit of this expression as $\eta \to 0^+$. The second integral on the right-hand side of Eq. (54) may be shown to vanish in this limit, upon making the substitution $q = p/\eta^2$ for any $\eta > 0$ and employing a series expansion of the integrand in powers of $\eta$. Thus,

$$\lim_{\eta\to 0^+}\frac{\partial \Theta}{\partial \eta} = \frac{1}{\pi^{1/2}}\int_0^\infty \frac{\Theta_w(\xi-p)-\Theta_w(\xi)}{p^{3/2}}dp. \tag{55}$$

In view of boundary conditions (49) and (51), the integral in Eq. (55) is zero whenever $\xi$ takes a value corresponding to a location on one of the vertical walls of the cell. This yields an integral equation for $\Theta_w(\xi)$ on these two cell walls. For reasons made evident below, the accurate numerical solution of this integral equation is a matter of some subtlety.

### A. Calculation of the wall temperature distribution

Again following Jimenez and Zufiria, we first separate out a square-root behavior of $\Theta_w(\xi)$ downstream of the leading corner (and its symmetric counterpart); this behavior arises from the parabolic nature of the diffusion equation (47) in the presence of an abrupt change in the wall boundary conditions. Thus, we write

$$\Theta_w(\xi) = 1 - A(\xi - l_1)^{1/2} - \theta(\xi - l_1) \quad \text{for } l_1 < \xi < l_1 + l_2 = \tfrac{1}{2}L, \tag{56}$$

$$\Theta_w(\xi) = A\left(\xi - l_1 - \tfrac{1}{2}L\right)^{1/2} + \theta\left(\xi - l_1 - \tfrac{1}{2}L\right) \quad \text{for } \tfrac{1}{2}L + l_1 < \xi < L, \tag{57}$$

where the constant $A$ and the smooth function $\theta(\tau)$ are to be determined, subject to $\theta(\tau) = o(\tau^{1/2})$ as $\tau \to 0$. By applying the no-flux boundary condition on $l_1 < \xi < l_1 + l_2$ and using Eqs. (55) and (56), we arrive at the following equation to be solved for $A$ and $\theta$ [cf. Eq. (25) in Jimenez and Zufiria[1]]:

$$0 = \pi A - \frac{2}{\xi^{1/2}} + \frac{2\theta(\tau)}{\tau^{1/2}} - \int_0^{\tau} \frac{\theta(\tau-\phi)-\theta(\tau)}{\phi^{3/2}} d\phi + \int_{\xi}^{\infty} \frac{\Theta_w(\xi-\phi)}{\phi^{3/2}} d\phi, \tag{58}$$

where, for convenience, we have introduced $\tau=\xi-l_1$ (hence $0<\tau<l_2$).

The last integral in Eq. (58) is evaluated by considering the contributions made from each wall on each passage of $\xi-\phi$ around the cell boundary; $\Theta_w(\xi)$ is known on the upper and lower cell walls and is given in terms of the unknowns $A$ and $\theta(\tau)$ on the vertical walls by Eqs. (56) and (57). To this end, we write

$$\int_{\xi}^{\infty} \frac{\Theta_w(\xi-\phi)}{\phi^{3/2}} d\phi = \sum_{m=1}^{\infty} \int_0^{L} \frac{\Theta_w(\phi)}{(\xi-\phi+mL)^{3/2}} d\phi \equiv \sum_{m=1}^{\infty} J_m. \tag{59}$$

Note that this shows up a minor typographical error in Jimenez and Zufiria's Eq. (26), where $\tau$ incorrectly appears in the denominator of the second integrand *in lieu* of $\xi$. By separating $J_m$ into components arising from each cell wall, we see that

$$J_m = \frac{2}{\left[\xi+\left(m+\frac{1}{2}\right)L\right]^{1/2}} - \frac{2}{(\xi+mL)^{1/2}} + \left\{ -\frac{2l_2^{1/2}}{(\tau-l_2+mL)^{1/2}} + 2\sin^{-1}\left[\frac{l_2^{1/2}}{(\tau+mL)^{1/2}}\right] + \frac{2l_2^{1/2}}{\left[\tau-l_2+\left(m-\frac{1}{2}\right)L\right]^{1/2}} - 2\sin^{-1}\left\{\frac{l_2^{1/2}}{\left[\tau+\left(m-\frac{1}{2}\right)L\right]^{1/2}}\right\}\right\} A - \int_0^{l_2} \frac{\theta(\phi)}{(\xi-\phi-l_1+mL)^{3/2}} d\phi + \int_0^{l_2} \frac{\theta(\phi)}{(\xi-\phi-2l_1-l_2+mL)^{3/2}} d\phi. \tag{60}$$

Thus, Eq. (58) may be written in the form of an integral equation for $A$ and $\theta(\tau)$, where the latter need be evaluated only in the interval $0\le\tau\le l_2$. It should be emphasized that the numerical solution of Eq. (58) benefits significantly from an interchange of the order of integration and summation, followed by the application of convergence acceleration techniques, as outlined in the Appendix. Jimenez and Zufiria[1] also commented on the need to employ convergence acceleration for various sums, but they did not record any technical details.

To solve Eq. (58) numerically, we introduce the $M+1$ grid points $\tau_m=ml_2/M$ for $m=0,1,\ldots,M$ and denote by $\theta_m$ the numerical approximation to $\theta(\tau_m)$ for $m=0,1,\ldots,M$. By construction, $\theta_0=0$. There are thus $M+1$ unknowns: $\theta_m$ for $m=1,2,\ldots,M$, together with $A$. We find it sufficient to perform all integrations using the trapezium rule (we have checked a sample of our results using Simpson's rule to confirm this). The equations to be solved are linear in each of the unknowns, which are readily determined by direct matrix inversion.

### B. Expressions for the normalized heat flux

Once $A$ and $\theta(\tau)$ have been computed, $\Theta_w(\xi)$ is known along the entire cell perimeter, and the normalized heat flux through the layer can be calculated. From Eqs. (44) and (45), it follows that the Nusselt number satisfies

$$\mathrm{Nu} \sim \frac{2k}{\varepsilon\pi} \int_0^{\infty} [\Theta(\xi,\eta)-\bar{T}] d\eta, \tag{61}$$

where $\xi$ is chosen to lie on wall II. Using Eq. (53) and the fact that

$$\frac{1}{\pi^{1/2}} \int_0^{\infty} \frac{\eta e^{-\eta^2/p}}{p^{3/2}} dp = 1, \tag{62}$$

we may rewrite the Nusselt number as

$$\mathrm{Nu} \sim \frac{2k}{\varepsilon\pi} \int_0^{\infty} \int_0^{\infty} \frac{\eta[\Theta_w(\xi-p)-\bar{T}]e^{-\eta^2/p}}{\pi^{1/2}p^{3/2}} dp\, d\eta. \tag{63}$$

Reversing the order of integration and carrying out the $\eta$ integration explicitly, we find that

$$\mathrm{Nu} \sim \frac{k}{\varepsilon\pi^{3/2}} \int_0^{\infty} \frac{\Theta_w(\xi-p)-\bar{T}}{p^{1/2}} dp \equiv \frac{k}{\varepsilon\pi^{3/2}} \mathcal{I}. \tag{64}$$

Although it is not immediately obvious from Eq. (64), this expression for Nu is independent of $\xi$ [as it must be asymptotically, according to Eq. (44)] provided that $\xi$ is chosen to lie on wall II. To verify this assertion, note that

$$\begin{aligned} \frac{d\mathcal{I}}{d\xi} &= \int_0^{\infty} \frac{1}{p^{1/2}} \frac{d}{d\xi} [\Theta_w(\xi-p)-\bar{T}] dp \\ &= -\int_0^{\infty} \frac{1}{p^{1/2}} \frac{d}{dp} [\Theta_w(\xi-p)-\Theta_w(\xi)] dp \\ &= -\left[\frac{\Theta_w(\xi-p)-\Theta_w(\xi)}{p^{1/2}}\right]_0^{\infty} - \frac{1}{2}\int_0^{\infty} \frac{\Theta_w(\xi-p)-\Theta_w(\xi)}{p^{3/2}} dp = 0, \end{aligned} \tag{65}$$

where the last equality follows from Eq. (55) and the no-flux boundary condition on this wall. Finally, we note from Eqs. (10), (11), and (64) that the large-Ra scaling factor between Nu and $\mathrm{Ra}^{1/3}$ in Eq. (9) is given by

$$C = \frac{(k\mathcal{I})^{4/3}}{\pi^2}. \tag{66}$$

The most straightforwardly computed contributions to the flux integral $\mathcal{I}$ are those from walls I and III (see Fig. 2). With an obvious notation, the sum of these contributions to the integral $\mathcal{I}$ defined in Eq. (64) is

$$\mathcal{I}_{\mathrm{I,III}} = \sum_{m=0}^{\infty} \int_0^{l_1} \frac{1}{2}(mL + \xi + p - l_1)^{-1/2} dp - \sum_{m=0}^{\infty} \int_0^{l_1} \frac{1}{2}(mL + \xi + p + l_2)^{-1/2} dp. \tag{67}$$

Now each of these integrals may be computed exactly, giving

$$\mathcal{I}_{\mathrm{I,III}} = \sum_{m=0}^{\infty} [(mL + \xi + p - l_1)^{1/2} - (mL + \xi + p + l_2)^{1/2}]. \tag{68}$$

Unfortunately this sum is not in a useful form for numerical evaluation, since its convergence relies on the cancellation between two terms, each of which grows with $m$. A more useful form is obtained by instead interchanging the orders of summation and integration and using the convergence acceleration formulas in the Appendix to obtain

$$\begin{aligned}\mathcal{I}_{\mathrm{I,III}} &= \frac{1}{2L^{1/2}} \int_0^{l_1} \left\{ \frac{1}{a^{1/2}} - \frac{1}{b^{1/2}} + \sum_{n=1}^{\infty} \binom{-\frac{1}{2}}{n} (a^n - b^n)\zeta(n+1/2) \right\} dp \\ &= \frac{1}{2} L^{1/2} \left[ 2a^{1/2} - 2b^{1/2} + \sum_{n=1}^{\infty} \binom{-\frac{1}{2}}{n} \left( \frac{a^{n+1}}{n+1} - \frac{b^{n+1}}{n+1} \right) \zeta(n+1/2) \right]_0^{l_1},\end{aligned} \tag{69}$$

where

$$a = \frac{\xi + p - l_1}{L}, \quad b = \frac{\xi + p + l_2}{L} = a + \frac{1}{2}, \tag{70}$$

and $\zeta$ is the Riemann zeta function.[39] Note that $l_1/L < a < \frac{1}{2}$ and $\frac{1}{2} + l_1/L < b < 1$. The sum in Eq. (69) converges geometrically, in contrast to the slower, algebraic convergence of Eq. (68). In fact, it makes for even better convergence if we write

$$\begin{aligned}\mathcal{I}_{\mathrm{I,III}} &= \frac{1}{2L^{1/2}} \int_0^{l_1} \left\{ \frac{1}{a^{1/2}} - \frac{1}{b^{1/2}} + \sum_{m=1}^{\infty} (m+1)^{-1/2} \times \sum_{n=0}^{\infty} \binom{-\frac{1}{2}}{n} \left[ \left( \frac{a-1}{m+1} \right)^n - \left( \frac{b-1}{m+1} \right)^n \right] \right\} dp \\ &= \frac{1}{2} L^{1/2} \left[ 2a^{1/2} - 2b^{1/2} + \sum_{n=1}^{\infty} \binom{-\frac{1}{2}}{n} \left[ \frac{(a-1)^{n+1}}{n+1} - \frac{(b-1)^{n+1}}{n+1} \right] [\zeta(n+1/2) - 1] \right]_0^{l_1}.\end{aligned} \tag{71}$$

The contributions from walls II and IV are rather more complicated to evaluate. We note that as $p$ increases from 0 to $\infty$, the first contribution to the integral $\mathcal{I}$ in Eq. (64) arises from the interval $0 < p < \xi - l_1$, corresponding to $\Theta_w(\xi - p)$ on the section of wall II leading back from $\xi$ to the corner between walls I and II. Thereafter, contributions to the integral arise from the intervals

$$\tfrac{1}{2}mL + \xi < p < \tfrac{1}{2}mL + \xi + l_2 \tag{72}$$

for $m = 1, 2, \ldots$, each interval corresponding to $\Theta_w(\xi - p)$ sweeping over wall II or IV in its entirety. Thus, we split the contribution from walls II and IV into two parts, respectively accounting for these two contributions,

$$\mathcal{I}_{\mathrm{II,IV}} = \mathcal{I}^0_{\mathrm{II,IV}} + \mathcal{I}^{\infty}_{\mathrm{II,IV}}. \tag{73}$$

We proceed by first considering

$$\mathcal{I}^{\infty}_{\mathrm{II,IV}} = \sum_{m=0}^{\infty} \int_0^{l_2} \frac{1/2 - A(l_2 - p)^{1/2} - \theta(l_2 - p)}{(mL + \xi + l_1 + l_2 + p)^{1/2}} - \frac{1/2 - A(l_2 - p)^{1/2} - \theta(l_2 - p)}{(mL + \xi + p)^{1/2}} dp. \tag{74}$$

There are clearly three types of contribution: first, a term independent of $A$ and $\theta$; second, a term proportional to $A$; and, third, a term involving $\theta$. The first term is readily evaluated by reversing the order of the summation and integration in Eq. (74), then applying convergence acceleration (see the Appendix) and finally integrating the resulting terms (similar to our treatment of $\mathcal{I}_{\mathrm{I,III}}$).

The second term, proportional to $A$, is

$$\mathcal{I}_A = A \sum_{m=0}^{\infty} \int_0^{l_2} \frac{(l_2 - p)^{1/2}}{(mL + \xi + p)^{1/2}} - \frac{(l_2 - p)^{1/2}}{(mL + \xi + l_1 + l_2 + p)^{1/2}} dp. \tag{75}$$

Since, for any positive constant $\alpha$,

$$\int_0^{l_2} \frac{(l_2 - p)^{1/2}}{(\alpha + p)^{1/2}} dp = \frac{\pi}{2}(\alpha + l_2) - \sqrt{\alpha l_2} - (\alpha + l_2)\tan^{-1}\sqrt{\frac{\alpha}{l_2}}, \tag{76}$$

we obtain

$$\mathcal{I}_A = A \sum_{m=0}^{\infty} [f_m(\xi) - f_m(\xi + L/2)], \tag{77}$$

where

$$f_m(\xi) = \frac{\pi}{2}(mL + \xi + l_2) - \sqrt{(mL + \xi) l_2} - (mL + \xi + l_2)\tan^{-1}\sqrt{\frac{mL + \xi}{l_2}}. \tag{78}$$

Direct numerical summation of Eq. (77) is rather problematic: although the summand is $O(m^{-3/2})$ for large $m$, accurate calculation of each term requires precise cancellation of terms that are themselves $O(m^{1/2})$ [if the straightforward cancellation of the even larger $O(m)$ terms is carried out manually]. To circumvent this problem, we sum the first few terms directly and replace the remaining terms by their large-$m$ expansion, giving an exact expression of the form

$$\mathcal{I}_A = A\sum_{m=0}^{M}[f_m(\xi) - f_m(\xi + L/2)] + A\sum_{m=M+1}^{\infty}\sum_{n=0}^{\infty} c_n m^{-3/2-n}. \tag{79}$$

The coefficients $c_n$ can be determined straightforwardly (for example, using a computer algebra package); the first few are

$$c_0 = \frac{l_2^{3/2}}{6L^{1/2}}, \quad c_1 = -\frac{l_2^{3/2}(5L + 8l_2 + 20\xi)}{80L^{3/2}}$$

and

$$c_2 = \frac{l_2^{3/2}}{L^{5/2}}\left[\frac{5\xi^2}{16} + \frac{(5L + 8l_2)\xi}{32} + \frac{84l_2L + 96l_2^2 + 35L^2}{1344}\right].$$

The double summation in Eq. (79) is then efficiently evaluated by reversing the order of summation, so that

$$\mathcal{I}_A = A\sum_{m=0}^{M}[f_m(\xi) - f_m(\xi + L/2)] + A\sum_{n=0}^{\infty} c_n\left[\zeta(n+3/2) - \sum_{m=1}^{M} m^{-n-3/2}\right], \tag{80}$$

which is rapidly convergent. A suitable value for $M$ is chosen by trial and error. (We use $M=10$ in our calculations, although the results are insensitive to this precise choice.)

The contribution to $\mathcal{I}^{\infty}_{\mathrm{II,IV}}$ from the terms involving $\theta$ is

$$\begin{aligned}\mathcal{I}_\theta &= \sum_{m=0}^{\infty}\int_0^{l_2}\theta(l_2 - p)\left[\frac{1}{(mL + \xi + p)^{1/2}} - \frac{1}{(mL + \xi + l_1 + l_2 + p)^{1/2}}\right]dp \\ &= \int_0^{l_2}\theta(l_2 - p)\frac{1}{L^{1/2}}\left(\frac{1}{a^{1/2}} - \frac{1}{b^{1/2}}\right)dp \\ &\quad + \int_0^{l_2}\theta(l_2 - p)\frac{1}{L^{1/2}}\sum_{m=1}^{\infty}\frac{1}{(m+1)^{1/2}} \\ &\quad \times \sum_{n=0}^{\infty}\binom{-\frac{1}{2}}{n}\left[\left(\frac{a-1}{m+1}\right)^n - \left(\frac{b-1}{m+1}\right)^n\right]dp,\end{aligned} \tag{81}$$

where in this expression

$$a = \frac{\xi + l_1 + l_2 + p}{L} = b + \frac{1}{2}, \quad b = \frac{\xi + p}{L}.$$

Evaluation of $\mathcal{I}_\theta$ is computationally time consuming since the sum in the second integral in Eq. (81) needs to be computed at each grid point.

Finally, the contribution $\mathcal{I}^0_{\mathrm{II,IV}}$ from the initial part of the integral, on wall II, is

$$\begin{aligned}\mathcal{I}^0_{\mathrm{II,IV}} &= \int_0^{\xi - l_1}\left[\frac{1}{2} - A(\xi - p - l_1)^{1/2} - \theta(\xi - p - l_1)\right]p^{-1/2}dp \\ &= (\xi - l_1)^{1/2} - \frac{1}{2}\pi A(\xi - l_1) - \int_0^{\xi - l_1}\theta(\xi - p - l_1)p^{-1/2}dp,\end{aligned} \tag{82}$$

which is readily computed once $\theta(\xi)$ and $A$ have been found from the numerical solution of the Childress cell problem. Combining the various contributions described above, we can calculate $\mathcal{I}$ in Eq. (64) and, hence, the coefficient $C$ in Eq. (66).

## VI. RESULTS

Next, we quantitatively compare results from our strongly nonlinear asymptotic theory to full numerical simulations of the 2D Oberbeck–Boussinesq equations (using the pseudospectral collocation method presented in Sec. III) at large Ra and $O(1)$ Pr. In Fig. 3, for example, the cell-edge temperature distribution obtained from a numerical simulation of Eqs. (1)–(3) at $\epsilon=0.01$ ($\mathrm{Ra}=10^6$), $k=\pi$, and $\mathrm{Pr}=1$ is compared to the corresponding prediction obtained from the solution to the Childress cell problem (also at $k=\pi$). The modest discrepancy between these curves is consistent with the appearance of $O(\varepsilon|\ln\varepsilon|)$ corrections in the higher-order expansion of $T(y,z)$ in the up- and downwelling plumes. The need for these corrections [which would have to be retained in, e.g., Eq. (33) if they were to be computed] is evident from a preliminary inspection of the inner viscous corner sublayers, not treated herein. We emphasize that, in the asymptotic

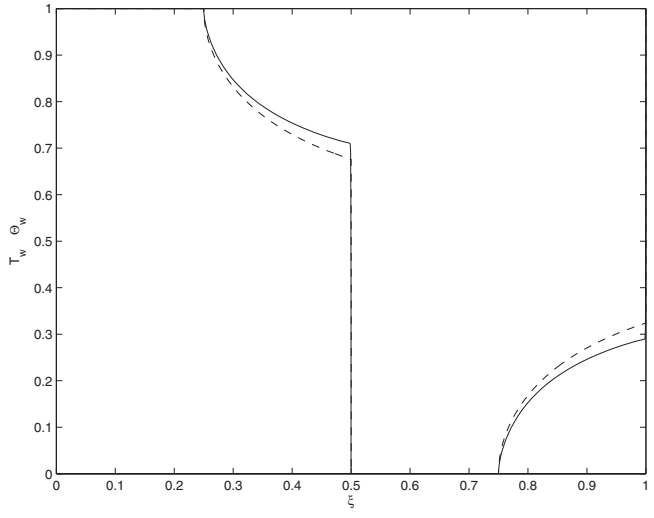


FIG. 3. Plot of cell-edge temperature distribution $T_w$ (solid curve) against stretched distance $\xi$ along the cell perimeter obtained from a full numerical simulation at $\epsilon=0.01$ ($\mathrm{Ra}=10^6$), $k=\pi$, and $\mathrm{Pr}=1$. The corresponding theoretical prediction ($\Theta_w$) is shown by the dashed curve.

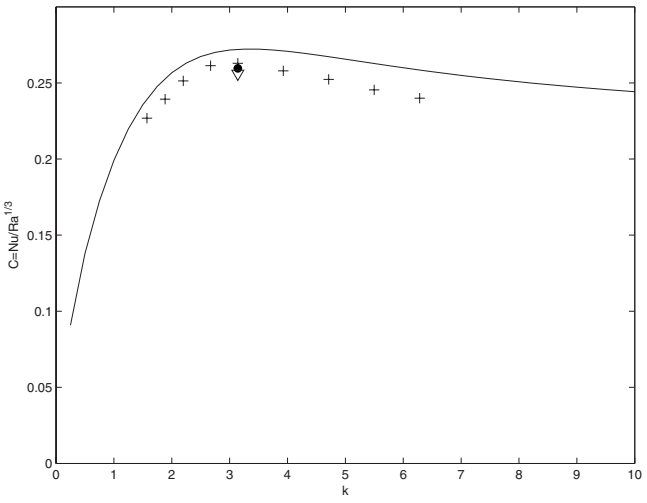


FIG. 4. Comparison of the coefficient $C$ in the asymptotic Nu-Ra relationship (9), as a function of cell wavenumber $k$, as obtained from: (1) the solution to the Childress cell problem using $m=800$ grid points (solid curve) and (2) full pseudospectral numerical simulations of Eqs. (1)–(3) for $10^6 \leq \mathrm{Ra} \leq 8\times 10^6$ and $\mathrm{Pr}=1$ (plus symbols), $\mathrm{Pr}=0.1$ (filled circle), and $\mathrm{Pr}=10$ (triangle). Note that the theoretical prediction is independent of Pr as $\mathrm{Ra}\to\infty$ for the given stress-free boundary conditions. A maximum in this curve occurs at $k\approx\pi$, implying that for a given large Ra, the heat flux is maximized for cells having an $O(1)$ wavenumber.

limit $\varepsilon\to 0$, we believe that we have accurately determined the temperature distribution throughout the cell (i.e., including within the plumes) to $O(1)$.

Again considering the simulation carried out for $k=\pi$, $\mathrm{Pr}=1$, and $\epsilon=0.01$, we find that the numerical estimate of the coefficient $C$ in the Nu-Ra relation (9) is $C_n=\epsilon\,\mathrm{Nu}_n \approx 0.2629$, where the subscript denotes "numerical." This value agrees closely with the theoretically predicted $C \approx 0.2723$ obtained by solving the Childress cell problem defined in Sec. V and evaluating the heat flux quadrature (64) for $k=\pi$. In addition, the numerically observed value of the core vorticity $\hat{\Omega}_n(y=\pi/2k, z=-1/2)\approx 0.5322$ for the given parameter values; cf. Fig. 1. The corresponding theoretical estimate is obtained by substituting the theoretical prediction for $C$ into the relation $\hat{\Omega}=\sqrt{C}$ (derived in Sec. IV). This calculation gives $\hat{\Omega}\approx 0.5218$, which compares favorably with the result from the numerical simulation.

In Fig. 4, the coefficient $C$ in the Nu-Ra relation (9) is plotted against wavenumber $k$. The agreement between the large-Ra theoretical prediction (given by the solid curve) and numerical estimates of this coefficient (shown by the plus symbols) provides strong evidence for the quantitative validity of the theory, particularly in view of the difficulty of numerically obtaining steady solutions to Eqs. (1)–(3) at large Ra. Indeed, the fact that the estimates from the numerical simulations fall below the theoretical values is consistent with the thickness of the thermal boundary layers tending to zero as $\mathrm{Ra}\to\infty$. Note that the theoretical prediction is *independent* of Pr; that is, in Eq. (9), the proportionality coefficient $C=C(k)$, only. This feature of the theory is immediately evident from inspection of the Childress cell problem (47)–(51), which is explicitly independent of the Prandtl number. Physically, for the given stress-free boundary conditions, the velocity field that advects the temperature in the thermal boundary layers and plumes around the cell perimeter is determined, at leading order, by the cellular flow within the *interior* of the convection cell. In the large-Ra limit, with $\mathrm{Pr}=O(1)$, the flow in the vortex core is inviscid, and its intensity is controlled by global balances of energy and heat flux that, *in steady state*, are independent of Pr, as shown in Sec. IV. By contrast, in the presence of no-slip rather than stress-free boundaries, the flow in the thermal boundary layers at the top and bottom of the cell would be altered at leading order by viscous effects, leading to a dependence of $C$ on both $k$ and Pr in that case. This conclusion is consistent with (and, in fact, helps to explain physically) the results of earlier theoretical and numerical studies of Rayleigh–Bénard convection with *stress-free* boundaries by Robinson,[11] Veronis,[17] and Moore and Weiss,[18] who also noted negligible Pr dependence in their Nu-Ra scaling relationships.

Both the asymptotic analysis and the numerical simulations suggest that *if* the most energetic contribution to thermal convection at large Ra occurs at a wavenumber that maximizes the heat flux through the layer, then the preferred wavenumber $k_m\approx\pi$, i.e., an $O(1)$ value (cf. Fig. 4). This prediction is consistent with the intuition that neither very long wavelength cells nor very narrow cells are favored energetically, both yielding lower net heat transport than cells with an $O(1)$ aspect ratio.

Somewhat surprisingly, however, the coefficient $C$ does not appear to tend to zero at large $k$ (see Fig. 4). This prediction may be understood by noting that the area of very narrow cells tends to zero as $k\to\infty$; in contrast, as $k\to 0$, the area of each cell tends to infinity. Thus, in the latter scenario, the energy dissipation in the (large) core dominates energy production in the thin plumes, which do not increase in size with decreasing $k$. In the former case, the dissipation in the core tends to zero, since the cell area vanishes. Evidently, the weak production of energy in the plumes, which also must tend to zero, is able to keep pace with the energy dissipation in this limit, so the flux remains finite and asymptotes to a constant value. Of course, the asymptotic solutions obtained in this investigation cease to be physically meaningful when the dissipation in the core no longer dominates that occurring in the viscous layers; that is why, for the solutions considered here, the dissipation does *not* grow as $k\to\infty$.

## VII. CONCLUSIONS

Using matched asymptotic analysis, we have analyzed steady 2D Rayleigh–Bénard convection in the limit of asymptotically large Ra and finite Pr. Our results yield a semianalytical description of strongly nonlinear convective states, providing a useful complement to the more common weakly nonlinear theories of convection. The analysis described here applies to convection with $O(1)$ values of both the wavenumber $k$ and Prandtl number Pr. Our results extend prior work on both long-wavelength convection and fast, but very viscous, convection. (Unfortunately, in view of the right-hand side of Eq. (2), our results for finite Pr do not apply for infinite Pr.[1]) In the former case, the leading-order

temperature *gradient* is not altered by the convection, while in the latter the flow in the vortex core is dominated by viscous rather than inertial effects. The flows investigated here completely homogenize the temperature and vorticity distributions in the interior of each convection cell and exhibit full coupling between the temperature and momentum fields. Unlike the case of constant-heat-flux thermal convection investigated in Ref. 12, the magnitude of the core vorticity is a function of cell width when constant-temperature boundary conditions are imposed. Moreover, the temperature jump across the thermal boundary layers is $O(1)$, rather than asymptotically small, in the fixed-temperature case.

The matched asymptotic analysis described in Sec. IV reduces the nonlinear boundary value problem governing steady 2D convection to a one-dimensional integral equation for the cell-edge temperature distribution. As discussed in Sec. V, the numerical solution of this integral equation requires care to treat singularities at the cell corners induced by the boundary conditions and to evaluate numerous slowly converging infinite sums of quadratures. With the cell-edge temperature distribution known, the Nusselt number can be obtained by careful evaluation of a further quadrature. In this way, our large-Ra asymptotic theory not only predicts that $\mathrm{Nu}\sim C\mathrm{Ra}^{1/3}$ but also furnishes a quantitative estimate of the proportionality coefficient $C$. This coefficient is shown to be a function only of the cell wavenumber $k$; specifically, $C$ is independent of Pr for the given stress-free boundary conditions. Full pseudospectral numerical simulations carried out for $\mathrm{Ra}=O(10^6)$, $\mathrm{Pr}=O(0.1-10)$ and a range of wavenumbers $k$ corroborate the asymptotic predictions.

The steady 2D convective states that we investigate undoubtedly are unstable in the large-Ra limit. Thus, it may be of interest and, in fact, feasible to perform a semianalytical secondary stability investigation, since the governing equations can be quasilinearized using the known form of the leading-order stream function. More significant, perhaps, is the understanding that unstable solutions, such as those investigated here, may play an important role in the fully turbulent dynamics that are physically realizable. This idea has been propounded by numerous authors—recently, by Waleffe,[40] Wedin and Kerswell,[2] Kawahara and Kida,[41] and others in the context of wall-bounded turbulent shear flows. Further support for the physical relevance of flows such as those analyzed here is provided by the recent large-eddy simulations of turbulent Langmuir circulation, a wind- and wave-driven convective flow in the upper ocean, by Tejada-Martinez and Grosch.[42] When averaged in the downwind direction and in time, the downwind velocity component in their simulations, which plays a role analogous to that of the temperature field in Rayleigh–Bénard convection, exhibits a striking resemblance to the steady downwind-invariant asymptotic solutions obtained in Ref. 12. Finally, we note that Newell *et al.*[43] conjectured that transport in turbulent thermal convection may be dominated by the random occurrence of coherent events; the authors contend that these episodic events are closely related to laminar, nearly singular solutions of the governing equations in the weak dissipation limit, as considered here.

Whether or not our steady, strongly nonlinear solutions prove to be dynamically relevant, they have merit as a means of estimating or bounding the heat transport in high Rayleigh number thermal convection. Unlike bounds on transport obtained using modern variational approaches, our prediction of the Nusselt–Rayleigh number scaling relationship is obtained from a convection solution that asymptotically satisfies *all* of the *differential* conservation constraints. Moreover, as indicated above, our analysis furnishes a quantitative estimate of the coefficient $C(k)$ in the Nusselt–Rayleigh number scaling relationship, thereby complementing the predictions of upper-bound theories. Ultimately, we hope that these two approaches may be fruitfully combined by employing asymptotic techniques similar to those described in this work to find near-optimal solutions of the nonlinear partial-differential eigenvalue problems arising in upper-bound analyses of various forms of convection.

## ACKNOWLEDGMENTS

G.P.C. gratefully acknowledges funding from NSF CAREER Award No. 0348981.

## APPENDIX: CONVERGENCE ACCELERATION

We record here useful results which we employed to accelerate the convergence of the various series in Eqs. (59) and (64).

### 1. First sum

One sum that arises repeatedly takes the form

$$\mathcal{S}_1=\sum_{m=1}^{\infty}\left[\frac{1}{(a+m)^{1/2}}-\frac{1}{(b+m)^{1/2}}\right],$$

where $|a|, |b|<1$. The terms in this sum decay algebraically, proportional to $m^{-3/2}$, so direct summation is undesirable. Instead, it is better to use the binomial expansions for $(a+m)^{-1/2}=m^{-1/2}(1+a/m)^{-1/2}$, and similarly for $(b+m)^{-1/2}$, to write

$$\begin{aligned}\mathcal{S}_1&=\sum_{m=1}^{\infty}m^{-1/2}\sum_{n=1}^{\infty}\binom{-\frac{1}{2}}{n}[(a/m)^n-(b/m)^n]\\&=\sum_{n=1}^{\infty}\binom{-\frac{1}{2}}{n}(a^n-b^n)\sum_{m=1}^{\infty}m^{-n-1/2}\\&=\sum_{n=1}^{\infty}\binom{-\frac{1}{2}}{n}(a^n-b^n)\zeta\left(n+\frac{1}{2}\right),\end{aligned}\tag{A1}$$

where $\zeta$ is the Riemann zeta function.[39] Since $\zeta(n+\frac{1}{2})\sim 1+(\frac{1}{2})^{n+1/2}$ as $n\to\infty$, we expect geometric convergence in Eq. (A1). Indeed, the convergence may be further improved by explicitly computing the sum of the first few terms in $\mathcal{S}_1$, writing instead

$$\mathcal{S}_1 = s_1 + \cdots + s_M + \sum_{m=M+1}^{\infty} s_m$$
$$= \sum_{m=1}^{M} s_m + \sum_{n=1}^{\infty} \binom{-\frac{1}{2}}{n} (a^n - b^n) \sum_{m=M+1}^{\infty} m^{-n-1/2}$$
$$= \sum_{m=1}^{M} s_m + \sum_{n=1}^{\infty} \binom{-\frac{1}{2}}{n} (a^n - b^n) \times \left[ \zeta\left(n+\frac{1}{2}\right) - 1 - \left(\frac{1}{2}\right)^{n+1/2} - \cdots - \left(\frac{1}{M}\right)^{n+1/2} \right]. \tag{A2}$$

The convergence is improved, since

$$\zeta\left(n+\frac{1}{2}\right) - 1 - \left(\frac{1}{2}\right)^{n+1/2} - \cdots - \left(\frac{1}{M}\right)^{n+1/2} \sim \frac{1}{(M+1)^{n+1/2}}.$$

When $0<a$, $b<2$, some adjustment to the argument above is required, so that we first write $(a+m)^{-1/2} = (m+1)^{-1/2}[1+(a-1)/(m+1)]^{-1/2}$ before constructing the binomial expansion (likewise for $b$) to yield

$$\mathcal{S}_1 = \sum_{n=1}^{\infty} \binom{-\frac{1}{2}}{n} [(a-1)^n - (b-1)^n] \left[ \zeta\left(n+\frac{1}{2}\right) - 1 \right]. \tag{A3}$$

Convergence may be further improved by explicitly summing the first few terms as in Eq. (A2).

Similar considerations apply to sums that we encounter of the form

$$\mathcal{S}_2 = \sum_{m=1}^{\infty} (p+m)^{-3/2} \equiv \sum_{m=1}^{\infty} c_m \tag{A4}$$

for $|p|<1$, so that

$$\mathcal{S}_2 = \sum_{n=0}^{\infty} \binom{-\frac{3}{2}}{n} p^n \zeta(n+3/2),$$

which converges geometrically. Convergence again may be accelerated further using

$$\mathcal{S}_2 = \sum_{m=1}^{M} c_m + \sum_{n=0}^{\infty} \binom{-\frac{3}{2}}{n} p^n \left[ \zeta\left(n+\tfrac{3}{2}\right) - 1 - \left(\frac{1}{2}\right)^{n+3/2} - \cdots - \left(\frac{1}{M}\right)^{n+3/2} \right]. \tag{A5}$$

Note that, in principle, we may directly evaluate the sum in Eq. (A4), since $\mathcal{S}_2$ is readily written as the generalized zeta function[39] $\mathcal{S}_2 = \zeta(3/2, p+1)$.

Another sum takes the form

$$\mathcal{S}_3 = \sum_{m=1}^{\infty} a_m, \tag{A6}$$

where

$$a_m = \frac{\mu}{(p-q+m)^{1/2}} - \sin^{-1}\frac{\mu}{(p+m)^{1/2}} \tag{A7}$$

for some constants $\mu, p, q$. Here we introduce terms $b_m$ with the same large-$m$ asymptotic form as $a_m$, but whose exact sum is known. Thus, we write

$$\mathcal{S}_3 = \sum_{m=1}^{\infty} a_m = \sum_{m=1}^{\infty} (a_m + b_m - b_m) = \sum_{m=1}^{\infty} b_m + \sum_{m=1}^{\infty} (a_m - b_m).$$

This reformulation is useful because the first sum is (by choice) known, and the second sum converges more rapidly than does $\mathcal{S}_3$ in the form (A6). The more terms we include in $b_m$, the better the convergence of the resulting sum of $a_m - b_m$. We find

$$a_m \sim \mu m^{-3/2}\left[\tfrac{1}{2}q - \tfrac{1}{6}\mu\right] + \mu m^{-5/2}\left[\tfrac{3}{8}q(q-2p) + \tfrac{1}{4}\mu^2 p - \tfrac{3}{40}\mu^4\right] + \mu m^{-7/2}\left[\tfrac{5}{16}q(q^2 - 3pq + 3p^2) - \tfrac{5}{16}p^2\mu^2 - \tfrac{3}{16}p\mu^4 - \tfrac{5}{112}\mu^6\right] \tag{A8}$$

$$\equiv \mu m^{-3/2} a_{m3} + \mu m^{-5/2} a_{m5} + \mu m^{-7/2} a_{m7}. \tag{A9}$$

Thus

$$\mathcal{S}_3 = \mu a_{m3}\zeta(3/2) + \mu a_{m5}\zeta(5/2) + \mu a_{m7}\zeta(7/2) + \sum_{m=1}^{\infty} \{a_m - \mu m^{-3/2} a_{m3} - \mu m^{-5/2} a_{m5} - \mu m^{-7/2} a_{m7}\}.$$

The summands in this expression are of order $m^{-9/2}$, and thus the error in truncating the sum at finite $m=M$ is $O(M^{-7/2})$. Additional terms in Eq. (A9) could be taken to further improve the rate of convergence.

Finally, for sums of the form

$$\mathcal{S}_4 = \sum_{m=1}^{\infty} \left[ \sin^{-1}\frac{\mu^{1/2}}{(a+m)^{1/2}} - \sin^{-1}\frac{\mu^{1/2}}{(b+m)^{1/2}} \right] \equiv \sum_{m=1}^{\infty} g_m,$$

we note the following large-$m$ expansion:

$$g_m \sim \tfrac{1}{2}\mu^{1/2} m^{-3/2}(b-a) - \tfrac{1}{8}\mu^{1/2} m^{-5/2}(b-a)(3a+3b-2\mu) + \tfrac{1}{16}\mu^{1/2} m^{-7/2}(b-a)[5a^2 + 5ab + 5b^2 - 5(b+a)\mu + 3\mu^2] \equiv \mu^{1/2}(m^{-3/2} g_{m3} + m^{-5/2} g_{m5} + m^{-7/2} g_{m7}).$$

Thus,

$$\mathcal{S}_4 = \mu^{1/2}\{g_{m3}\zeta(3/2) + g_{m5}\zeta(5/2) + g_{m7}\zeta(7/2)\} + \sum_{m=1}^{\infty}\{g_m - \mu^{1/2}m^{-3/2}g_{m3} - \mu^{1/2}m^{-5/2}g_{m5} - \mu^{1/2}m^{-7/2}g_{m7}\}.$$


[1] J. Jimenez and J. A. Zufiria, "A boundary-layer analysis of Rayleigh–Bénard convection at large Rayleigh number," J. Fluid Mech. **178**, 53 (1987).
[2] H. Wedin and R. Kerswell, "Exact coherent structures in pipe flow: Travelling wave solutions," J. Fluid Mech. **508**, 333 (2004).
[3] J. A. Domaradzki and R. W. Metcalfe, "Direct simulations of the effects of shear on turbulent Rayleigh–Bénard convection," J. Fluid Mech. **193**, 499 (1988).
[4] A. C. Poje and J. L. Lumley, "A model for large scale structures in turbulent shear flows," J. Fluid Mech. **285**, 349 (1995).
[5] K. Chandra, "Instability of fluids heated from below," Proc. R. Soc. London, Ser. A **164**, 216 (1937).
[6] F. H. Busse, M. A. Richards, and A. Lenardic, "A simple model of high Prandtl and high Rayleigh number convection bounded by thin low-viscosity layers," Geophys. J. Int. **164**, 160 (2006).
[7] G. O. Roberts, "Fast viscous Bénard convection," Geophys. Astrophys. Fluid Dyn. **12**, 235 (1979).
[8] P. Olson and G. M. Corcos, "A boundary layer model for mantle convection with surface plates," Geophys. J. R. Astron. Soc. **62**, 195 (1980).
[9] P. B. Rhines and W. R. Young, "How fast is a passive scalar mixed within closed streamlines?" J. Fluid Mech. **133**, 133 (1983).
[10] A. F. Pillow, Australian Department of Supply Aeronautical Research Laboratories, Technical Report No. A.79, 1952.
[11] J. L. Robinson, "Finite amplitude convection cells," J. Fluid Mech. **30**, 577 (1967).
[12] G. P. Chini, "Strongly nonlinear Langmuir circulation and Rayleigh–Bénard convection," J. Fluid Mech. **614**, 39 (2008).
[13] H. Johnston and C. R. Doering, "Comparison of turbulent thermal convection between conditions of constant temperature and constant flux," Phys. Rev. Lett. **102**, 064501 (2009).
[14] T. Y. Chu and R. J. Golstein, "Turbulent convection in a horizontal layer of water," J. Fluid Mech. **60**, 141 (1973).
[15] J. R. Herring, "Investigation of problems in thermal convection," J. Atmos. Sci. **20**, 325 (1963).
[16] J. R. Herring, "Some analytic results in the theory of thermal convection," J. Atmos. Sci. **23**, 672 (1966).
[17] G. Veronis, "Large-amplitude Bénard convection," J. Fluid Mech. **26**, 49 (1966).
[18] D. R. Moore and N. O. Weiss, "Two-dimensional Rayleigh–Bénard convection," J. Fluid Mech. **58**, 289 (1973).
[19] F. Heslot, B. Castaing, and A. Libchaber, "Transition to turbulence in helium gas," Phys. Rev. A **36**, 5870 (1987).
[20] E. E. DeLuca, J. Werne, R. Rosner, and F. Cattaneo, "Numerical simulations of soft and hard turbulence: Preliminary results for two-dimensional convection," Phys. Rev. Lett. **64**, 2370 (1990).
[21] B. I. Shraiman and E. D. Siggia, "Heat transport in high-Rayleigh-number convection," Phys. Rev. A **42**, 3650 (1990).
[22] X.-Z. Wu and A. Libchaber, "Scaling relations in thermal turbulence: The aspect-ratio dependence," Phys. Rev. A **45**, 842 (1992).
[23] R. M. Kerr, "Rayleigh number scaling in thermal convection," J. Fluid Mech. **310**, 139 (1996).
[24] R. M. Kerr and J. R. Herring, "Prandtl number dependence of Nusselt number in direct numerical simulations," J. Fluid Mech. **419**, 325 (2000).
[25] L. N. Howard, "Heat transport by turbulent convection," J. Fluid Mech. **17**, 405 (1963).
[26] C. R. Doering and P. Constantin, "Variational bounds on energy dissipation in incompressible flows. III. Convection," Phys. Rev. E **53**, 5957 (1996).
[27] R. R. Kerswell, "New results in the variational approach to turbulent Boussinesq convection," Phys. Fluids **13**, 192 (2001).
[28] C. R. Doering, F. Otto, and M. Reznikoff, "Bounds on vertical heat transport for infinite-Prandtl-number Rayleigh–Bénard convection," J. Fluid Mech. **560**, 229 (2006).
[29] F. H. Busse, "Non-linear properties of thermal convection," Rep. Prog. Phys. **41**, 1929 (1978).
[30] G. Amati, K. Koal, F. Massaioli, K. R. Sreenivasan, and R. Verzicco, "Turbulent thermal convection at high Rayleigh numbers for a Boussinesq fluid of constant Prandtl number," Phys. Fluids **17**, 121701 (2005).
[31] L. N. Trefethen, *Spectral Methods in Matlab* (SIAM, Philadelphia, 2000).
[32] S. Childress, "Alpha-effect in flux ropes and sheets," Phys. Earth Planet. Inter. **20**, 172 (1979).
[33] G. K. Batchelor, "On steady laminar flow with closed streamlines at large Reynolds number," J. Fluid Mech. **1**, 177 (1956).
[34] A. M. Soward, "Fast dynamo action in a steady flow," J. Fluid Mech. **180**, 267 (1987).
[35] S. Chandrasekhar, *Hydrodynamic and Hydromagnetic Stability* (Dover, New York, 1981).
[36] S. Childress and A. Gilbert, *Stretch, Twist and Fold: The Fast Dynamo*, Lecture Notes in Physics (Springer, New York, 1995).
[37] J. F. Harper, "On boundary layers in two-dimensional flow with vorticity," J. Fluid Mech. **17**, 141 (1963).
[38] G. K. Batchelor, *An Introduction to Fluid Dynamics* (Cambridge University Press, Cambridge, 1967).
[39] E. T. Whittaker and G. N. Watson, *A Course of Modern Analysis*, 4th ed. (Cambridge University Press, Cambridge, 1927).
[40] F. Waleffe, "Exact coherent structures in channel flow," J. Fluid Mech. **435**, 93 (2001).
[41] G. Kawahara and S. Kida, "Periodic motion embedded in plane Couette turbulence: Regeneration cycle and burst," J. Fluid Mech. **449**, 291 (2001).
[42] A. E. Tejada-Martinez and C. E. Grosch, "Langmuir turbulence in shallow water. Part 2. Large-eddy simulation," J. Fluid Mech. **576**, 63 (2007).
[43] A. C. Newell, D. A. Rand, and D. Russell, "Turbulent transport and the random occurrence of coherent events," Physica D **33**, 281 (1988).